Materials and Structures (2025) 58:230
https://doi.org/10.1617/s11527-025-02757-z

ORIGINAL ARTICLE

RILEM TC 294-MPA: interlaboratory study of the mechanical properties of fiber-reinforced ground granulated blast furnace slag-based alkali-activated concrete

Arkamitra Kar · Pujitha Ganapathi Chottemada · Lucija Hanžič · J. S. Kalyana Rama · Patricia Kara De Maeijer · Behzad Nematollahi · Kruthi Kiran Ramagiri · Laura Rossi · Aljoša Šajna · Shizhe Zhang · Mingzhong Zhang · Guang Ye · Frank Dehn

Received: 21 April 2025 / Revised: 25 July 2025 / Accepted: 2 August 2025

Abstract Under the directives of the RILEM Technical Committee 294-MPA, this publication reports on the findings of an interlaboratory study that tested fiber-reinforced GGBFS-based alkali-activated concrete (FRAAC), with participants from Belgium, India and Slovenia. The research also elaborates prediction models for the tensile splitting strength of GGBFS-based FRAAC. This research endeavoured between 2020 and 2024 to find a globally reproducible FRAAC mix that could attain the required mechanical strength and workability criteria. The primary goal of the interlaboratory study was to generate FRAAC without the use of superplasticizers in order to maintain an S4 class consistency slump and achieve the desired 28-days cube compressive strength of 40 MPa. Steel and PVA fibers were determined to be incorporated to the GGBFS-based AAC mix at 0.3 and 0.1% volume fractions, respectively, through iterative interlaboratory investigations. Experimental program was conducted to examine the compressive and tensile splitting strength of these FRAAC combinations at different curing ages, ranging from 1 to 720 days. The findings indicate that while there were a few interlaboratory variations in the mechanical properties, the FRAAC produced was uniform across all participants. The desired compressive strength of 40 MPa was attained by GGBFS-based FRAAC with both steel and PVA fibers at 28 days. Although FRAAC containing steel fibers exhibited the higher

RILEM TC footnote
This study was performed within the framework of the RILEM TC 294-MPA "Mechanical properties of alkali-activated concrete" by Interlaboratory Study expert group 6 (ILS6) from February 2022 to February 2024. This TC Report was internally reviewed and approved by the RILEM TC 294-MPA Active Members by 18th April 2025 that concluded its activities on 27th September 2024.
The final list of TC Active members for TC Report (as on 25/07/2025):
TC 294-MPA Chair: Guang Ye
TC 294-MPA Deputy Chair: Frank Dehn

Active TC Members: Elijah Damilola Adesanya, Rahul Attupurathu Vijayan, Susan Bernal Lopez, Farid Benboudjema, Jelle Bezemer, Maria Chiara Bignozzi, Choi Lin Chan, Boyu Chen, Ozlem Cizer, Xiaodi Dai, Vinh Dao, Geert De Schutter, Frank Dehn, Brice Delsaute, Vilma Ducman, Pujitha Ganapathi Chottemada, Meng Gao, Luise Gobel, Lucija Hanzic, Zhangli Hu, Yuyan Huang, Kazuo Ichimiya, Sri Kalyana Rama Jyosyula, Muralidhar Kamath, Fragkoulis Kanavaris, Arkamitra Kar, Patricia Kara De Maeijer, Arno Keulen, Albina Kostiuchenko, Sreejith Krishnan, Pavel Kryvenko, Maite Lacante, Georgy Lazorenko, Ning Li, Zhenming Li, Tianshi Lu, Mladena Lukovic, Tero Luukkonen, Yang Lv, Yuwei Ma, Alastair Marsh, Giulia Masi, Stijn Matthys, Luiz Miranda de Lima, Shravan Muthukrishnan, Mariya Nedeljkovic, Behzad Nematollahi, Kolawole A. Olonade, Marta Palacios, Majda Pavlin, Quoc Tri Phung, John L. Provis, Francisca Puertas Maroto, Zhenxu Qian, Zhengyao Qu, Kruthi Kiran Ramagiri, Jesus Rodriguez-Sanchez, Laura Rossi, Aljosa Sajna, Marco Sirotti, Wei Sha, Caijun Shi, Stephanie Staquet, Beibei Sun, Yubo Sun, Yaxin Tao, Babak Vafaei, Jannie S. J. Van Deventer, Xiaomei Wan, Frank Winnefeld, Jean Noel Yankwa Djobo, Guang Ye, Hailong

Published online: 23 August 2025

early compressive strength, FRAAC prepared with steel and FRAAC prepared with PVA both demonstrated a 720-days compressive strength of about 61 MPa. The FRAAC mixes with steel fiber additions exhibited a tensile splitting strength that was approximately 30% higher than the mix with PVA fibers. Nonetheless, at all ages, the tensile splitting strength of both FRAAC mixes was clearly higher than 2 MPa. These results support reliable and consistent experimental findings, which allude towards FRAAC as a sustainable substitute for conventional Portland cement concrete.

Keywords Fiber reinforced alkali-activated concrete (FRAAC) · Ground granulated blast furnace slag (GGBFS) · Mechanical properties · Prediction models

1 Introduction

Current estimates indicate the annual production of Portland cement (PC) as 4.1 billion metric tonnes [1], contributing to 12–15% of industrial energy consumption and around 8% of global CO_2 emissions [2]. The World Green Building Council [3] outlines a goal to achieve at least 40% less embodied carbon in all new construction, infrastructure, and renovations by 2030. It is therefore necessary to explore PC alternatives to improve the sustainability of concrete. The mechanical [4–6] and microstructural [7, 8] characteristics of alkali-activated concrete (AAC), along with environmental benefits, suggest that it could be an alternative to Portland cement concrete (PCC). However, further investigation is required on the long-term mechanical performance of AAC [9]. Life cycle assessments (LCAs) show that AAC can mitigate greenhouse gas emissions by around 70%, water demand by 25%, energy consumption by about 40%, and other environmental toxicity indicators by 22–94% depending on the mixture proportions [10, 11]. Industrial waste or by-products like ground granulated blast furnace slag (GGFBS) is frequently used as precursor for AAC production, making it both environmentally and economically viable [12]. The long-term mechanical strength of GGBFS-based AAC degrades due to microcracks that form as a result of drying and autogenous shrinkage [13, 14]. The brittle and inelastic nature of the AAC matrix and the interfacial transition zone (ITZ) between this matrix and the aggregate reduces the tensile strength of AAC and increases its tendency to cracking [11, 15]. Hence, different

Ye, Kangting Yin, Juho Yliniemi, Zengliang Yue, Minzhong Zhang, Shizhe Zhang, Zuhua Zhang, Zhengning Zhou, Xiaohong Zhu, Lea Zibret and Yibing Zuo.

A. Kar (✉) · P. G. Chottemada
Department of Civil Engineering, Birla Institute of Technology and Science (BITS)-Pilani, Hyderabad Campus, Hyderabad, Telangana 500 078, India
e-mail: arkamitra.kar@hyderabad.bits-pilani.ac.in

L. Hanžič · A. Šajna
Zavod za gradbeništvo (ZAG) Slovenije, Slovenian National Building and Civil Engineering Institute, 1000 Ljubljana, Slovenia

J. S. Kalyana Rama
Department of Civil Engineering, Mahindra University, Survey No: 62/1A, Bahadurpally, Jeedimetla, Hyderabad, Telangana 500043, India

P. Kara De Maeijer
Faculty of Applied Engineering, University of Antwerp, 2020 Antwerp, Belgium

B. Nematollahi
Department of Civil and Structural Engineering, The University of Sheffield, Sheffield S10 2TN, UK

K. K. Ramagiri
Department of Civil Engineering, Indian Institute of Technology Hyderabad, IITH Road, Sangareddy, Kandi, Hyderabad, Telangana 502 285, India

L. Rossi · F. Dehn
Institute of Concrete Structures and Building Materials (IMB), Karlsruhe Institute of Technology (KIT), 76131 Karlsruhe, Germany

S. Zhang · G. Ye
Group Concrete Modelling and Materials Behavior, Microlab/Section Materials and Environment, Department of 3MD, Faculty of Civil Engineering and Geosciences, Delft University of Technology, Stevinweg 1, 2628 CN Delft, The Netherlands

S. Zhang
Renewi Mineralz & Water, Vlasweg 12, 4782 PW Moerdijk, The Netherlands

M. Zhang
Department of Civil, Environmental and Geomatic Engineering, University College London, London WC1E 6BT, UK

types of fiber reinforcements have been widely used in AACs to enhance their tensile and flexural characteristics [14–16] and improve mechanical and crack-bridging capabilities [15, 17–23]. Hence, to promote its practical applications globally, extensive research needs to be conducted on the long-term mechanical properties of fiber-reinforced AAC (FRAAC).

Under ambient conditions, AAC produced with GGBFS as the sole binder yielded a compressive strength of 79.87 MPa, a tensile splitting strength of 5.52 MPa, and a flexural strength of 5.93 MPa [24]. The development and connectivity of microcracks as a result of unreacted binder residues cause the flexural strength of GGBFS-based AACs to decrease by about 13% over a period of 90 to 540 days [13]. Furthermore, alkali-activated binders (AABs) are susceptible to crack development due to the significantly lower amount of chemically bonded and interstitial water [17, 25]. This phenomenon is more pronounced in GGBFS-based AABs [26, 27]. To address the above issues fiber reinforcements are widely acknowledged as an effective method [28].

Addition of fibers such as steel, polypropylene, polyvinyl alcohol (PVA), basalt and glass enhances the ductility in AACs [29, 30]. The addition of polypropylene or PVA fibers, however, has the significant disadvantage of increasing the viscosity of the freshly mixed concrete [29–34]. In alkali-activated mortars, PVA fibers (> 0.5%) demonstrated the greatest decrease in flow compared to basalt and steel fibers due to their ability to adsorb water [35, 36]. Superplasticizers have frequently been added to the concrete mixes to solve this issue [37]. The impact of superplasticizers, which were initially intended for PCC, on the chemistry of AACs necessitates more research and is beyond the purview of this work. Hence, the current study focuses on formulating workable FRAAC without the use of superplasticizers because of the related costs and uncertainty.

The mechanical properties of FRAAC are influenced by various properties including the fiber material and geometry. The intrinsic fiber properties, fiber–matrix interface bonding, and fiber content also show significant influence on FRAAC properties [38]. Steel fibers are widely employed as reinforcements in concrete structures because of their high ductility, strength, and availability [39]. Regardless of the fiber geometry, the incorporation of steel fibers into GGBFS-based AAC resulted in a significant increase in compressive, splitting tensile, and flexural strength values [40–42]. This is mostly explained by the tendency of steel fibers to prevent the expansion of fractures, reduce stresses within fractures, and delay the crack propagation by redistributing them [42]. According to previous research [43], it was found that FRAAC reinforced with up to 0.6% PVA fibers exhibited enhancements in the 28-days flexural and tensile splitting strength by up to 11% and 18%, respectively. However, the corresponding workability was reduced by up to 36% on addition of these fibers.

A recent study correlated the modulus of elasticity, compressive, splitting tensile, flexural and residual flexural strength of steel fiber reinforced AAC with the compressive strength of plain AAC, the fiber volume fraction and the fiber reinforcing index [44]. In another study on GGBFS-based FRAAC with steel fiber reinforcement, the volume of fibers and the 28-day cylinder compressive strength were presented as the two parameters in a multivariable linear regression model for predicting the strength under splitting tension [45]. Limited reports are available on proposed equations for compression, splitting tension and elastic modulus of FRAACs using fibers other than steel [46, 47]. One such study employing basalt, steel, and polypropylene fibers in fly ash-GGBFS blended AACs proposed models to predict the compressive and tensile splitting strengths based on the compressive strength of plain mix, fiber volume, and fiber type [48]. Nonetheless, further investigation is necessary to develop prediction models for mechanical strength of various FRAACs at varying ages.

This paper presents the results of an interlaboratory study involving participants from Belgium, India, and Slovenia, testing GGBFS-based FRAAC. The research findings indicate limited reports on the long-term strength of plain AAC, and no reports are published till date on the long-term strength of FRAACs. No systematic reports or standard codes of practice are presently available on fiber-reinforced AACs. Additionally, the reduction in workability of the concrete mixture due to the addition of fibers is either compromised or overcome by the addition of superplasticizers. However, the influence of this addition on the chemistry of AACs is yet unknown. As previous studies exhibited promising outcomes with the incorporation of steel and PVA fibers on the mechanical properties of AAC, the present study evaluates the long-term strength of FRAACs with

different proportions of steel and PVA fibers, without the addition of superplasticizers to produce a workable mixture with maximum strength benefits. The specific objectives are, (i) to produce ambient-cured FRAACs, (ii) to evaluate the mechanical strength of the FRAAC mixes by conducting compressive and tensile splitting strength tests ranging from 1 to 720 days, (iii) to develop statistical models for predicting the tensile splitting strength of FRAACs for different testing ages.

2 Materials and methods

The experimental procedure was designed as an Inter-laboratory Study and performed by three participants. Each participant produced and tested their own specimens using aggregate with a maximum grain size of up to 20 mm, GGBFS as a precursor and the aqueous solution of sodium hydroxide and sodium silicate as an activator.

2.1 Properties of constituents

Aggregates were composed of locally sourced aggregate fractions available to the respective participants. The principal aggregate characteristics, namely type of aggregate, oven-dried particle density, saturated surface-dried density and water absorption after 24 h are summarized in Table 1. Aggregates grading is shown in Fig. 1 as cumulative particle size distribution. The aggregates were conditioned in a laboratory and were in an ambient-dry state before use.

The GGBFS from two sources was used, namely from ASTRAA Chemicals (India) and EcoCem Benelux B.V. (Ireland). Physical properties, such as average particle diameter, surface area, fineness and density, as well as chemical composition are summarized in Tables 2 and 3, respectively.

The aqueous solution of sodium hydroxide and sodium silicate was prepared before mixing the FRAAC. First, a day before mixing, the NaOH pellets were dissolved in water and since the dissociation to Na^+ and OH^- ions is an exothermic reaction the solution was left to cool to the ambient temperature. Next, about half an hour before mixing, the aqueous solution of sodium silicate was added to the dissolved NaOH. The brand and properties of the sodium silicate solution are shown in Table 4. Since the content of SiO_2 and Na_2O in sodium silicate differs depending on the brand, the amount of NaOH pellets was calculated by fixing the ratio between SiO_2, Na^+ and GGBFS and by fixing the volume ratio between paste and aggregate.

Two types of fibres were used in the study, namely steel and synthetic, polyvinyl alcohol (PVA) fibres. The selection of fibres and their dosage was based on the target 28-day cube compressive strength of 40 MPa and S4 slump class requirements as per BS 8500-1:2015 [51]. Fiber properties are summarized in Table 5. Steel fibers are exposed to the possibility of corrosion in low alkaline systems. PVA fibers are non-corrosive. Hence, this study employs both type of fibers to identify their respective effects on mechanical properties of FRAAC.

2.2 Mixture proportions and specimens preparation

The objective of the RILEM TC 294-MPA ILSILS6 expert group was to obtain GGBFS-based FRAAC mixtures with the following characteristics: (a) to avoid the use of superplasticizers (SP) as there are no conclusive reports on the chemistry of reactions between the fibers and the SP; (b) to achieve a slump

Table 1 Type of aggregate and their properties, where WA_{24} stands for water absorption within 24 h. All properties were measured according to EN 1097-6 [49]

Participant	Fine aggregates properties			Coarse aggregates properties		
	Type	Density (kg L^{-1})	WA_{24} (wt%)	Type	Specific gravity	WA_{24} (wt%)
1	River sand	2.65	0.5	Crushed granite	2.72	0.1
2	Limestone/dolomite river sand	2.71	0.9	Limestone/dolomite river gravel	2.74	0.6
3	River sand	2.65	0.5	Crushed porphyry	2.72	0.1

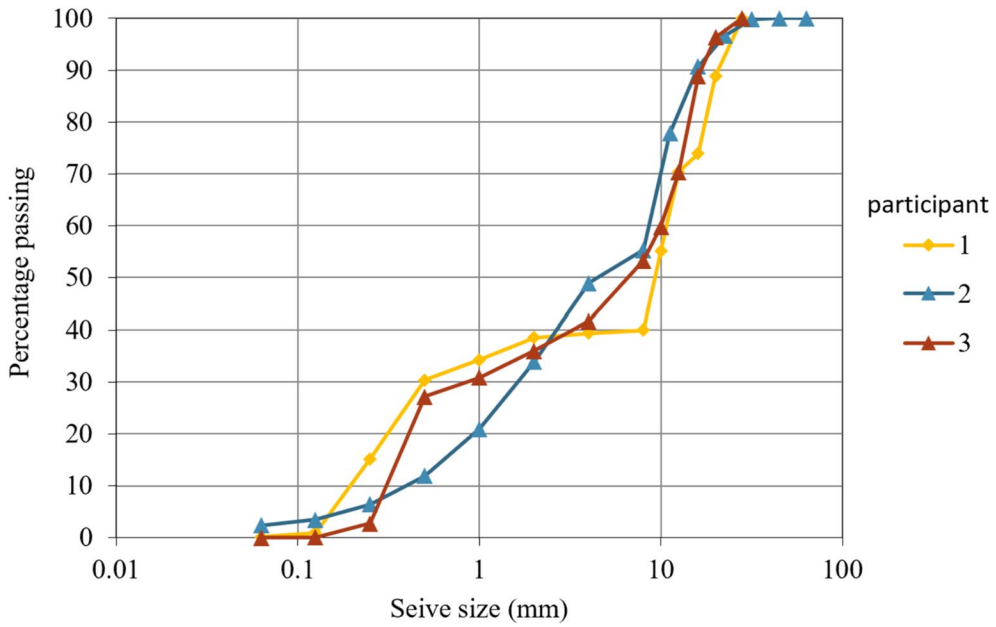

Fig. 1 Particle size distribution of aggregate

Table 2 Physical properties of GGBFS, where d_{50} stands for average particle diameter corresponding to the cumulative frequency of 50 wt%

Participant	GGBFS source	d_{50} (μm)	Blaine fineness [m^2/kg]	Density [kg/m^3]
1	ASTRAA chemicals (India)	13.93	390	2850
2, 3	EcoCem Benelux B.V. (Ireland)	11	450	2910

Table 3 Chemical composition of GGBFS

Participant	GGBFS chemical compositions (wt. % as oxide)*									LOI (%)
	CaO	SiO_2	Al_2O_3	MgO	SO_3	Fe_2O_3	TiO_2	K_2O	Na_2O	
1	38.31	35.64	17.15	7.73	0.18	0.55	0.00	0.05	0.14	0.25
2	41.86	34.55	10.77	9.11	1.22	0.50	0.63	0.35	0.64	–
3	39.51	36.61	12.30	7.39	0.68	0.63	0.00	0.48	0.36	1.48

*Labs 2 and 3 used 2 different batches of GGBFS from Ecocem

Table 4 Brand and properties of sodium silicate (Na_2SiO_3) solution

Properties of sodium silicate	1	2	3
Brand	PQ Corporation	Woellner Geosil 34417 [50]	PQ Corporation
Density (kg L^{-1})	1.530	1.552	1.535
SiO_2 content (wt%)	29.4	27.5	29.7
Na_2O content (wt%)	14.7	16.9	14.8

Table 5 Properties of steel and PVA fibers

Participant	1		2,3	3
Fiber type	Steel (hooked-end)	PVA	Steel (hooked-end)	PVA
Brand	Vaishnav composites		Bekaert Dramix ®	Kuralon REC15/8
Density (kg L^{-1})	7.85	1.29	8.03	1.3
Length (mm)	30	12	35	8
Diameter (µm)	500	22	550	40
Aspect ratio	60	545	65	–
Elongation (%)	0.5–3.5	4.0–9.0	0.8	6.5
Initial modulus of elasticity (GPa)	210	25.2	200	–
Tensile strength (MPa)	1276	1600	1345	1600

Table 6 FRAAC mix design is based on ILS1 GGBFS-based AAC (M2) [53] mix design with addition of steel or PVA fibers

Precursor (GGBFS) [kg/m^3]	450
Na_2O wt% of GGBFS	4.3
SiO_2 wt% of GGBFS	4.3
H_2O wt% of GGBFS	46
Dry sand (0/4) [kg/m^3]	645
Dry aggregates (4/20) [kg/m^3]	967
Fibers steel/PVA [% vol of FRAAC]	0.3/0.1

of around 180–200 mm corresponding to the S4 slump class requirements of BS 8500-1:2015 [51]; (c) to achieve a 28-day cube compressive strength of 40 MPa; and (d) to focus on the flexural and tensile characteristics. Based on four rounds of initial trials conducted by Participant 1 and subsequent validation by Participant 3, the proportions of fibers in the FRAAC mixtures were decided as 0.3% steel and 0.1% PVA to achieve the objectives of this RILEM TC 294-MPA ILS6 expert group.

The composition of FRAAC is summarized in Table 6.

Mixing of the components was performed in the laboratory horizontal pan mixers with a capacity of 50 L, thus several batches were needed to prepare all the specimens. It was ensured that the specimens corresponding to each type of test (compression or splitting tensile) for each fiber type (steel or PVA) were cast in the same batch. The number of available moulds was also a limiting factor which necessitated spreading out the specimen preparation over several days. The mixing procedure was as follows:

The alkaline activator is prepared 24 h before the concrete mixing procedure to ensure the sodium hydroxide pellets dissolve completely. This process entails the combination of solid NaOH with half of the necessary water for the mixture, which is then allowed to settle to ambient temperature over the course of several hours. Within this timeframe, the NaOH solution typically attains ambient temperature. In order to optimize efficacy, it is recommended that a two-part activator be prepared at the beginning of the day (Part I) and sodium silicate be added after the solution has sufficiently cooled by the end of the day (Part II).

- **Part I:** The procedure begins with the dissolution of a specific quantity of NaOH pellets in water ("to add") for the mix. If a commercial NaOH solution is available, it is recommended that you proceed to Part II. Pellets are introduced into an empty plastic laboratory container, which is then followed by water. The container is sealed securely to prevent mass loss. After vigorous stirring, the solution is let to cool. The temperature typically stabilizes at approximately 60 °C. The solution is typically available for use the following day if it is prepared the day before. The empty container is weighed to ensure precision, and it is subsequently re-weighed with a solution of NaOH and water. A subsequent measurement is taken the following day to corroborate the precise total mass of water and NaOH. Any loss of mass is prevented by immediate wrapping following the addition of water.

- **Part II:** The following day, specified quantity of sodium silicate solution is weighed and added to the same container that is already filled with the previously prepared solution of dissolved and cooled NaOH and water. It is then thoroughly mixed and allowed to cool. At a temperature of 20 ± 2 °C, the cooling duration for both Part I and Part II in a single container typically falls within the range of 60 to 90 min. The actual cooling time, however, is contingent upon the laboratory conditions, regional climate, and seasonal factors. It is imperative to document the temperature and relative humidity (RH) during the mixing procedure.
- The sieved aggregates are firstly introduced to the mixer. Crushed coarse aggregates such as granite, porphyry or basalt, and fine aggregates (sand), together with the precursor (GGBFS) were mixed for approximately 1 min;
- Fibers were added in three portions, each being 1/3 of the total fibre quantity. Each portion was mixed at least for 30 s to achieve a uniform distribution and fibre coating before the next portion was added.
- Activator (aqueous solution of NaOH and sodium silicate) was then added and mixed for 30 s;
- The remaining water was added, and mixing continued for 3 to 5 min until a homogenous, workable mix was obtained.

Immediately after mixing was completed, the slump test was performed to check the consistency of FRAAC as a measure of workability. The specimens for mechanical testing were prepared by casting the FRAAC mix into the plastic standard moulds and compacting the material on the vibration table for approximately 30 s. The moulds were covered with plastic and stored at laboratory conditions until demoulding. It was found that, approximately 24 h after casting, the specimens were often too soft for de-moulding; therefore, de-moulding took place after 2 days. This is possibly due to the presence of the fibers hindering the reaction between the water in the activator and the precursor. However, for specimens subjected to testing at an early age of 1 day, demoulding was done after 24 h of casting. After de-moulding, the specimens were tightly enclosed with cling film and stored at laboratory conditions until testing. An overview of specimens manufactured by three participants is given in Tables 7 and 8.

2.3 Test methods

The slump test was performed according to EN 12350-2 [54] standard. The measurement was rounded to the nearest 10 mm. At least two test repetitions were made.

The mechanical performance of the FRAAC was determined through compressive, flexural and

Table 7 Summary of steel and PVA GGBFS-based FRAAC specimen dimensions

Test	Participant ID	1		2	3	
		Steel	PVA	Steel	Steel	PVA
Compression	Cu-Cube	Cu-150 mm		Cu-150 mm	Cu-100 mm	
Tensile splitting	Cy-Cylinder	Cy-Ø 150mm, h 300 mm			–	

Table 8 Summary of the number of GGBFS-based FRAAC specimens casted and tested at the various ages by each participant, where N stands for the number of specimens, Cu/Cy indicates the specimen type, followed by the age of testing

Participant	1		2	3	
Test	Steel	PVA	Steel	Steel	PVA
Compression	No. = 24; Cu: 1, 3, 7, 28, 90, 180, 360, 720 d	N = 24; Cu: 1, 3, 7, 28, 90, 180, 360, 720 d	N = 12; Cu: 3, 7, 28, 90 d	N = 21; Cu: 1, 7, 28, 90, 180, 360, 570 d	N = 21; Cu: 1, 7, 28, 90, 180, 360, 570 d
Tensile splitting	N = 24; Cy: 1, 3, 7, 28, 90, 180, 360, 720 d	N = 24; Cy: 1, 3, 7, 28, 90, 180, 360, 720 d	N = 12; Cu: 3, 7, 28, 90 d	–	–

splitting strength tests. The density of the specimens was measured just before the mechanical test was conducted. Specimens were tested at the same facility as they were fabricated. A set of at least three specimens was tested for various ages ranging from 1 to 720 days after casting. To check for the inter-batch variations, a 28-day compression test was performed on a set of specimens from each batch by participant 2.

The density of the specimens was determined according to standard EN 12390-1 [55] and EN 12390-7 [56]. Specimens were checked for any shape irregularities and their mass was measured. The volume was calculated using the specified dimensions for cubic specimens, while for cylinders and prisms, it was determined based on their measured dimensions.

The compressive strength test, performed in compliance with the standard EN 12390-3 [57], using cubic specimens with dimensions of 100 mm × 100 mm × 100 mm or 150 mm × 150 mm × 150 mm at the ages of 1, 3, 7, 28, 90, 180, 360, and 720 days. A reduction factor of 0.95 for compressive strength was applied to cube specimens with dimensions of 100 mm × 100 mm × 100 mm to convert it to equivalent cube strengths [58]. The specimens were loaded at the rate of 0.6 ± 0.2 MPa/s.

The tensile splitting test was conducted as per standard EN 12390-6 [59] on either cubic with dimensions 150 mm × 150 mm × 150 mm or cylindrical specimens with dimensions of 150 mm × 300 mm at the ages of 1, 3, 7, 28, 90, 180, 360, and 720 days. The load was applied at a rate between 0.04 to 0.06 MPa/s. The ILS6 tests were conducted from February 2022 to July 2024.

3 Results and discussions

3.1 Slump test

The slump test on the GGBFS-based FRAAC mixes was performed by two participants and results are shown in Figs. 2 and 3.

Both 0.3SF and 0.1PVA mixes met the S4 class requirements of BS 8500-1:2015 [51]. However, with respect to the plain AAC mixture, the workability of 0.3SF was reduced by 16% and that of 0.1PVA was reduced by up to 32%. The slump for 0.3SF mix was 210 mm, while 0.1PVA mix had slump of 180 mm and 170 mm, indicating 19%

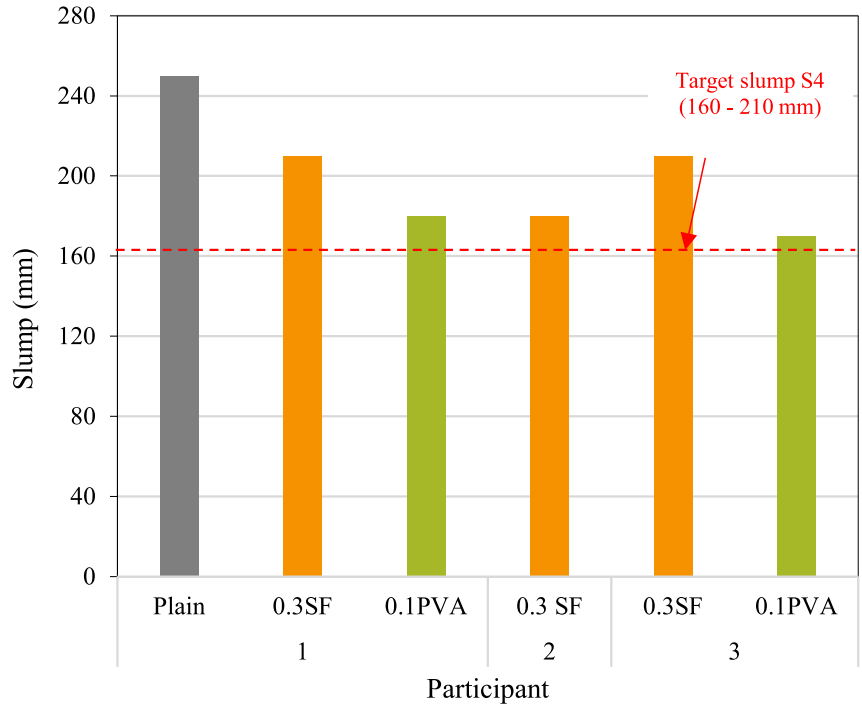

Fig. 2 Slump test results of the GGBFS-based FRAAC mixes tested for ILS6

Fig. 3 Slump test performed by participants 1, 2, and 3

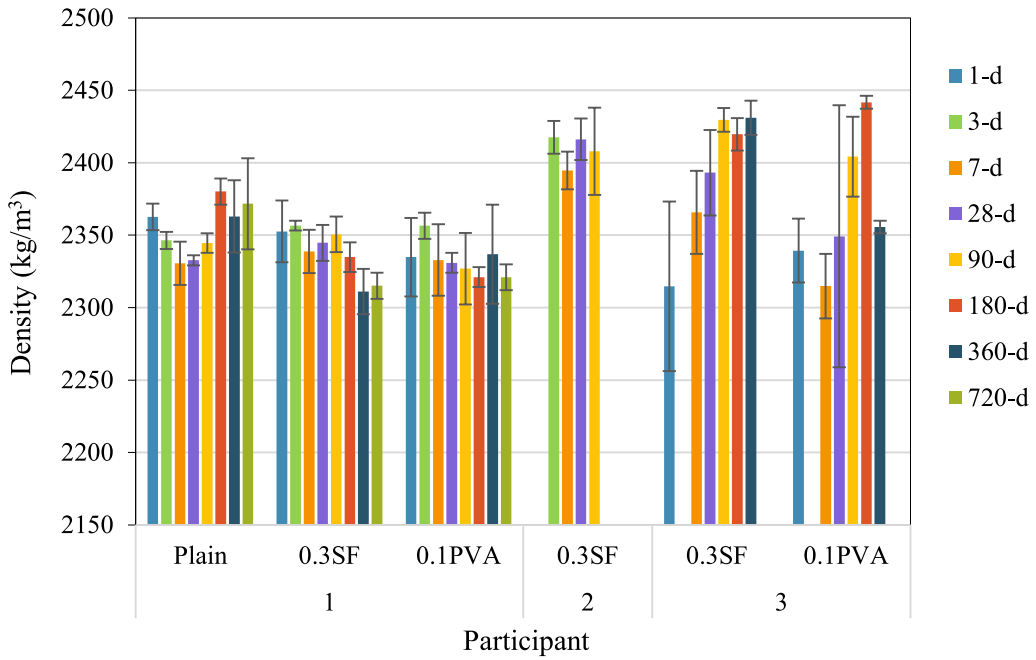

Fig. 4 Density of hardened GGBFS-based FRAAC with steel and PVA fibers

lower workability for 0.1PVA. Despite the higher steel fiber content in 0.3SF, it had greater workability than that of 0.1PVA, due to water-absorbing nature of PVA fibers, which hinders the flow of FRAAC. Thus, the addition of PVA fibers was limited to 0.1% for the ILS6 tests to meet S4 slump criteria. It is hypothesised that, the good workability of the mixtures, even at higher dosages of steel fibers, can be due to their tendency of lesser agglomeration, subject to further validation as future scope of this study.

3.2 Densities of hardened GGBFS-based specimens

The densities of the different GGBFS-based FRAAC specimens are shown in Fig. 4, measured over 1 to 720 days for three replicates. Participant 1 reported densities of plain AAC, 0.3SF and 0.1PVA mixes from 2310 to 2380 kg/m^3 at all ages, with less than 3% variation. Participant 2 reported 0.3SF densities between 2390 and 2420 kg/m^3 over 3 to 90 days, showing up to 1% variation. The marginal variations in density over different ages of testing indicate consistent mixing and controlled storage conditions. However, participant 3 observed greater density variations from 2310 to 2450 kg/m^3 for both 0.3SF and 0.1PVA, with 5% and 6% differences due to difficulty placing of specimens in the moulds during casting, in particular for 0.1PVA mixes. Overall, despite some variations, all specimens had densities between 2300 and 2450 kg/m^3, influenced by raw material properties, casting methods, temperature conditions.

3.3 Mechanical properties of hardened GGBFS-based specimens

3.3.1 Compressive strength

The compressive strength results of the GGBFS-based FRAAC tested by three participants as part of ILS6, are shown in Fig. 5. These results were recorded over 1 to 720 days for three replicate specimens. All participants achieved the target strength of 40 MPa at 28 days for both 0.3SF and 0.1PVA mixes. The compressive strength increased steadily up to 90 days, even after accounting for the different specimen size adopted by Participant 2.

Participant 1 reported 1-day compressive strength of 8 MPa for 0.3SF and 13 MPa for 0.1PVA, while participant 3 observed lower values about 5 MPa and 6 MPa respectively, for 0.3SF and 0.1PVA specimens. The low early compressive strength was due to incomplete development of the FRAAC matrix and the weak fiber–matrix bond creating a weak ITZ around the fiber leading to crack initiation. By 3 days, compressive strength exceeded 40 MPa for 0.3SF

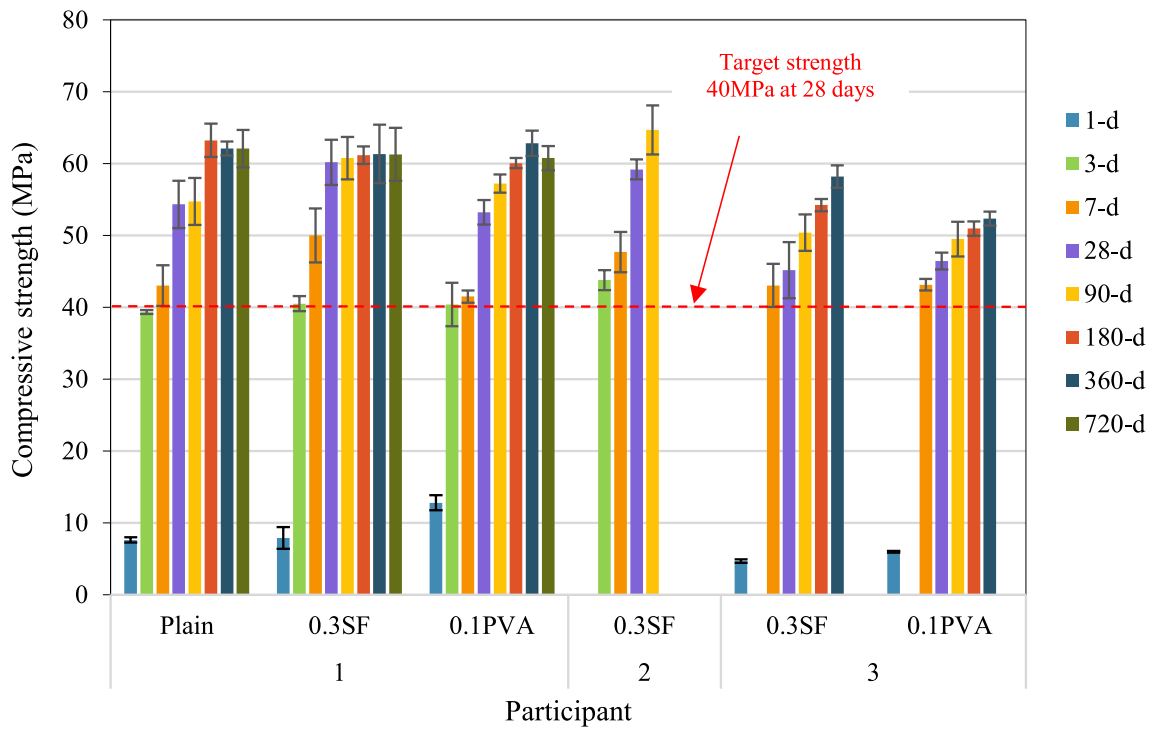

Fig. 5 Compressive strength of hardened GGBFS-based FRAAC with steel and PVA fibers

mixes, reaching 41 MPa for participant 1 and 44 MPa for participant 2. It is further noticed that the 7-days and 28-days compressive strength of all FRAAC specimens exceeds 40 MPa.

At 28 days, 0.3SF specimens showed compressive strength of around 60 MPa for both participants 1 and 2. The corresponding strength of 0.1PVA was 53 MPa as reported by participant 1. The strength of 0.3SF was about 11% higher than the corresponding plain AAC, while the strength of 0.1PVA was about 2% lower. This difference in strength is attributed to the better fiber–matrix bond development as demonstrated in a previous study [52], enhanced compaction and greater rigidity offered by the steel fibers in FRAAC. However, participant 3 reported a 28-days compressive strength of about 48 MPa for both the 0.3SF and 0.1PVA specimens.

There is no significant variation in the compressive strength results observed after 28 days for 0.3SF specimens tested by participant 1. However, a significant increase in strength of up to 29% was observed between the 28-days and 360-days results by participant 3. Meanwhile, a corresponding strength increase of up to 9% is reported by participant 2 for the 0.3SF specimens, up to 90 days. The 0.1PVA specimens, on the other hand, demonstrated up to 14% increase in strength until 720 days, and a 13% increase in strength up to 360 days, as reported by participants 1 and 3, respectively. By 720 days, both mixes reached approximately 61 MPa (participant 1), showing that steel fibers developed strong early bonding, but both mixes ultimately achieved similar long-term strength due to development of refined microstructure. Additionally, the compressive strength values of the FRAAC mixes match closely with the plain AAC, showing no overall influence of fibers on the compressive strength of AAC.

3.3.2 Tensile splitting strength

The tensile splitting strength results of FRAAC specimens tested by participants 1 and 2 are shown in Fig. 6. At 1 day, both 0.3SF and 0.1PVA had tensile splitting strength about 0.5 MPa (participant 1), which is about 66% less than the corresponding strength of plain AAC. This indicates increased number of weak zones in FRAAC specimens at early age, resulting in a weak matrix. This observation can also be attributed to the distribution of fibers and their orientation in the specimens. For 0.3SF, tensile splitting strength at 3, 7 and 28 days were about 3 MPa, 3.5 MPa and 4

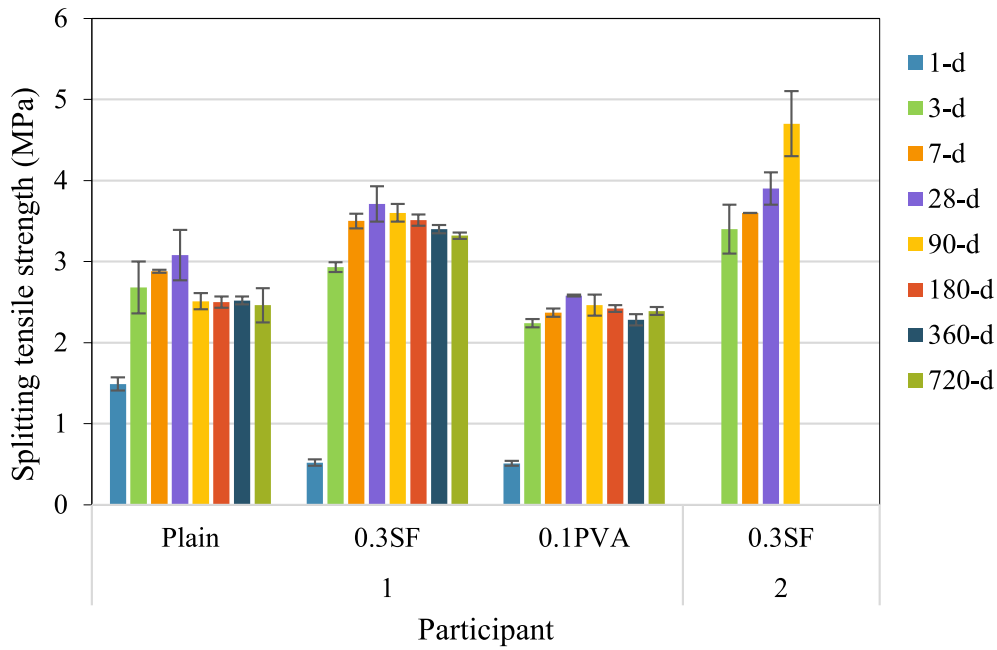

Fig. 6 Tensile splitting strength of hardened GGBFS-based FRAAC with steel and PVA fibers as part of ILS6

MPa, respectively, with consistent results between participants up to 28 days. However, at 90 days, participant 1 reported no significant change, while participant 2 observed a 21% increase in tensile splitting strength. This inconsistency in the results between the two participants could be mainly attributed to the variations in the development of the FRAAC matrix and the fiber–matrix bonding, due to different raw material properties and different environmental conditions. The possible source of this inconsistency can also be the fiber distribution in the samples and the matrix shrinkage.

The 28-day tensile splitting strength of 0.1PVA was observed to be about 2.6 MPa, which is approximately 16% lower than that of plain AAC according to the results by participant 1. However, the tensile splitting strength of 0.3SF is 20% higher than the corresponding plain mix. The significant difference in the tensile splitting strength results of the two FRAAC mixes is attributed to the greater tensile splitting strength, enhanced fiber–matrix bond. This aligns with previous studies [29, 30, 60] showing that the addition of fibers can only improve the tensile splitting strength when high dosage of short, stiff fibers is used. These fibers become activated by microcracks before the material reaches the failure stress. Participant 1 also observed an 11% reduction in tensile splitting strength for both mixes by 720-days, likely due to the increased formation of the calcium aluminosilicate hydrate (C–A–S–H) matrix as well as the occurrence of microcracks, which are mostly seen in GGBFS-based AAC as the reaction process progresses [13].

3.4 Prediction modelling

3.4.1 Prediction model for tensile splitting strength

Stepwise linear regression models were used to predict the tensile splitting strength from compressive strength of the FRAAC using experimental data. As there is only one dosage for each fiber, the tensile splitting strength is expressed only as function of the corresponding variation in compressive strength in this study. Hence, the equations proposed are valid only for the specific matrix and fiber types used in this study. As a follow up to this study, the models can be refined further with more extensive data from different labs or different raw materials when they become available.

3.4.1.1 0.3% Steel fibres (0.3SF) The proposed model for 0.3SF is as follows:

$$f_{sp} = 0.195\left(f_c'\right)^{0.714} \quad (1)$$

The 0.3SF mix model accurately predicts tensile splitting strength across various curing durations. The correlation between predicted and actual values is shown in Table 9 and Fig. 7.

The predicted values demonstrate good accuracy. This indicates the model effectively captures the relationship between compressive and tensile splitting strengths. The high coefficient of determination ($R^2 = 0.94$) indicates strong fit. An R^2 value close to 1 shows that 94% of the variability in tensile splitting strength can be explained by the model. The low mean absolute error (MAE) and Root mean square error (RMSE) values further validate the model's reliability. A small MAE (0.22) and RMSE (0.25)

Table 9 Experimental versus predicted tensile splitting strength for 0.3SF

Days	Compressive strength, MPa	Experimental tensile splitting strength, MPa (with standard deviation)	Predicted splitting tensile strength, MPa
1	7.89	0.51 (0.04)	0.85
3	40.52	2.93 (0.06)	2.74
7	50.01	3.5 (0.14)	3.19
28	60.19	3.71 (0.28)	3.64
90	60.77	3.7 (0.32)	3.66
180	61.18	3.51 (0.08)	3.68
360	61.35	3.4 (0.12)	3.69
720	61.29	3.32 (0.13)	3.68

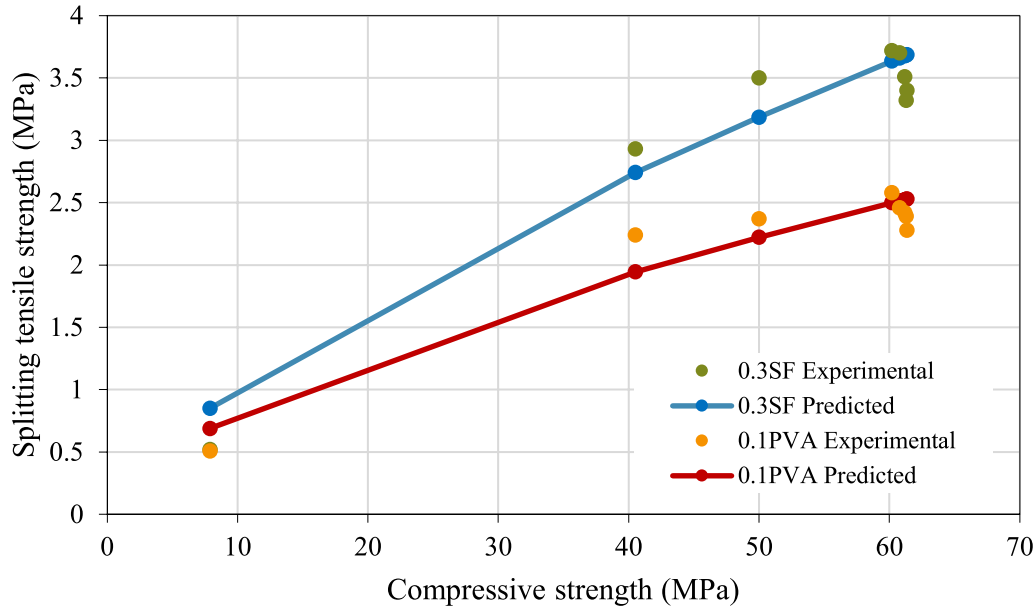

Fig. 7 Variation of tensile splitting strength with compressive strength values for GGBFS-based FRAAC with steel and PVA fibers

indicate that the model's predictions closely align with actual split tensile strength values.

3.4.1.2 0.1% PVA fibers (0.1PVA) The model proposed for 0.1PVA mix is:

$$f_{sp} = 0.186\left(f_c'\right)^{0.634} \quad (2)$$

The predictive model reveals a strong correlation between compressive and tensile splitting strengths for the 0.1PVA mix. These results are presented in Table 10 and Fig. 7.

The model demonstrates good predictive accuracy, as evidenced by an R^2 value of 0.93. The close alignment between predicted and actual tensile splitting strengths further underscores the model's effectiveness. A small MAE (0.16) and RMSE (0.17) indicate that the model's predictions closely align with actual tensile splitting strength values.

3.4.2 *Performance of prediction model for tensile splitting strength*

The results show that the proposed models are capable of accurately predicting the tensile splitting strength based on compressive strength for 0.3SF and 0.1PVA mixtures. These prediction models have satisfactory statistical performance, with R^2

Table 10 Experimental vs predicted tensile splitting strength for 0.1PVA

Days	Compressive strength, MPa	Experimental tensile splitting strength, MPa (with standard deviation)	Predicted splitting tensile strength, MPa
1	7.89	0.51 (0.03)	0.69
3	40.52	2.24 (0.05)	1.94
7	50.01	2.37 (0.15)	2.22
28	60.19	2.58 (0.08)	2.50
90	60.77	2.46 (0.06)	2.51
180	61.18	2.42 (0.10)	2.52
360	61.35	2.28 (0.11)	2.53
720	61.29	2.39 (0.13)	2.53

values surpassing 0.90, showing a significant connection between predicted and experimental values. This shows that the models explain a significant percentage of the variability in tensile splitting strength. Nonlinear regression is used to reflect the intricacy of the relation between compressive and tensile strength. The addition of steel or PVA fibers in the FRAAC matrix alters stress distribution during loading, contributing to the observed nonlinear behavior. The nonlinear exponents most likely result from the interplay of fiber pull-out, bridging, and matrix deformation. Initially, at lower levels of compressive strength, the impact of fibers on tensile strength may be minimal. However, as compressive strength increases, the reinforcing effect becomes more evident, emphasizing the importance of optimizing fiber content in practical applications.

There is a positive correlation between tensile splitting strength and curing duration (age) in both models (0.3SF and 0.1PVA). Compressive and tensile splitting strengths show improvement with age, indicating continued hydration and strength growth. Interestingly, both types of fibres show significant increases in tensile splitting strength throughout the first three days of curing when compared to their starting values. The fiber types also exhibit varying rates of growth in tensile splitting strength.

The 0.3SF model exhibits slightly better initial strength and a faster strength enhancement than the 0.1PVA model, implying that steel fibers play a substantial role in early-age strength. On day 28, systems with both fiber types attain their maximum tensile splitting strength, with steel fibers outperforming PVA fibers. This suggests that steel fibers are more successful at improving long-term tensile splitting strength. The models remain accurate for the specific mixture proportions used in this study at all the test ages; however, their practical utility can be enhanced through the generation and incorporation of relevant experimental data using varied mixture proportions and fiber types in different locations. The predicted strength growth rate steadily declines over time, which corresponds to typical cementitious material behaviour as hydration slows.

While the models are highly accurate for the tested formulations, their applicability to other types of binder composites requires additional validation. Future studies should seek to broaden the dataset to include a more diverse range of mix proportions and additives.

4 Conclusions

This paper presents the results of an interlaboratory study involving participants from Belgium, India, and Slovenia, testing fiber-reinforced GGBFS-based FRAAC. While fiber addition ($>0.3\%$ for steel and $>0.1\%$ for PVA) reduces workability, this is often mitigated by using superplasticizers, though their impact on FRAAC chemistry remains unclear. As a result, the fiber dosages adopted in this study are restricted to 0.3% for steel and 0.1% for PVA fibers. The purpose of adding PVA fibers was not to enhance the mechanical strength but to enhance the cracking resistance. Additionally, the PVA fibers can be used in combination with steel fibers and compensate for the disadvantages of steel fibers in a low alkaline environment. This paper evaluates the mechanical properties of FRAACs with steel and PVA fibers, without superplasticizers, to maximise strength while maintaining workability. The main research output can be summarized as follows:

- The slump test results showed that both 0.3SF and 0.1PVA mixes met the S4 class requirements. The 0.3SF had a higher slump of 210 mm compared to the 0.1PVA mix of 180 mm, reflecting 19% lower workability for the 0.1PVA mix.
- The GGBFS-based FRAAC mixes achieved the target compressive strength of 40 MPa at 28 days for both 0.3SF and 0.1PVA mixes, with continued compressive strength growth over time. While 0.3SF mix showed higher early compressive strength due to better fiber–matrix bonding and steel fiber rigidity, both mixes ultimately reached similar long-term average strengths of around 61 MPa by 720 days (though limited to one participant's results). The lower early compressive strength in 0.1PVA mixes was compensated by improved performance over time, attributed to reduced shrinkage and enhanced compaction from PVA fibers.
- The tensile splitting strength of GGBFS-based FRAAC mixes showed that 0.3SF mix had higher tensile strength than 0.1PVA mix, with a 30% difference at 28 days. Steel fibers enhanced the ten-

sile splitting strength due to better fiber–matrix bonding. The results were consistent up to 28 days, though some variation occurred at 90 days between participants, likely due to differences in material properties and long-term curing conditions. By 720 days, a slight reduction in tensile splitting strength was observed, probably due to the formation of microcracks and the C–A–S–H matrix in GGBFS-based FRAAC.

- The proposed models accurately predict splitting tensile strength based on compressive strength for 0.3SF and 0.1PVA mixes, with R2 values above 0.80, indicating strong correlation with experimental data. Nonlinear regression captures the complex relationship between compressive and tensile splitting strengths, influenced by fiber pull-out, bridging, and matrix deformation.

Acknowledgements The authors thank EcoCem Benelux B.V. (Ireland) for providing GGBFS for European ILS6 participants. The authors would also like to thank their respective institutes and organizations for providing the necessary resources to prepare this TC Report. LH and AŠ acknowledge the support of the Slovenian Research and Innovation Agency through research programme P2-0273.

Authors' contributions All authors contributed to this paper. The first draft of the manuscript was written by PGC, KKR, AK, LH and PKDM, was edited by PKDM, PGC, KKR, AK, LH, LR, and SZ, and was reviewed by KRJS, BN, AS, SZ, MZ, GY and FD. All authors read and approved the final manuscript.

Data Availability All data used in this study are presented in the manuscript.

Declarations

Conflict of interest This paper was prepared by the working ILS6 Expert group from RILEM Technical Committee 294-MPA. The authors have no conflicts of interest to declare that are relevant to the content of this paper. Provided results for ILS6 by participants are meant for publication in the journal of Materials and Structures as RILEM TC Report.

References

1. Cement production worldwide from 1995 to 2023 (2024). https://www.statista.com/statistics/1087115/global-cement-production-volume/. Accessed 2 Oct 2024
2. Meireles PDS, Pereira DSS, Melo MAF, Braga RM, Freitas JCO, Melo DMA, Silvestre FRS (2019) Technical evaluation of calcium sulphate α-hemihydrate in oilwell application: an alternative to reduce the environmental impacts of Portland cement. J Clean Prod 220:1215–1221. https://doi.org/10.1016/j.jclepro.2019.02.120
3. Bringing embodied carbon upfront: Coordinated action for the building and construction sector to tackle embodied carbon. The World Green Building Council's report, 2019. https://worldgbc.s3.eu-west-2.amazonaws.com/wp-content/uploads/2022/09/22123951/WorldGBC_Bringing_Embodied_Carbon_Upfront.pdf. Accessed on 2 Oct 2024
4. Provis JL (2018) Alkali-activated materials. Cem Concr Res 114:40–48. https://doi.org/10.1016/j.cemconres.2017.02.009
5. Rakhimova NR, Rakhimov RZ (2019) Literature review of advances in materials used in development of alkali-activated mortars, concretes, and composites. J Mater Civ Eng 31(11):03119002. https://doi.org/10.1061/(ASCE)MT.1943-5533.0002899
6. Ramagiri KK (2021) Evaluation of high-temperature, bond, and shrinkage of alkali-activated binder concrete. Ph.D. thesis submitted to Birla Institute of Technology and Science (BITS)-Pilani, Hyderabad Campus, Telangana, India, October 2022
7. Garcia-Lodeiro I, Taboada VC, Fernández-Jiménez A, Palomo Á (2017) Recycling industrial by-products in hybrid cements: mechanical and microstructure characterization. Waste Biomass Valor 8(5):1433–1440. https://doi.org/10.1007/s12649-016-9679-x
8. Gebregziabiher BS, Thomas R, Peethamparan S (2015) Very early-age reaction kinetics and microstructural development in alkali-activated slag. Cem Concr Compos 55:91–102. https://doi.org/10.1016/j.cemconcomp.2014.09.001
9. Kara De Maeijer P, Ramagiri KK, Luković M, Rossi L, Masi G, Kar A, Ganapathi Chottemada P, Yliniemi J, Ichimiya K, Sha W, Dehn F, Ye G Chapter 7. Hardened AAM properties. In: Ye G, Dehn F (eds) Mechanical properties of alkali-activated concrete. RILEM State-of-the-Art Reports. Springer (in submission)
10. Worrell E, Price L, Martin N, Hendriks C, Meida LO (2011) Carbon dioxide emissions from the global cement industry. Annu Rev Energy Environ 26:303–329. https://doi.org/10.1146/annurev.energy.26.1.303
11. Jiang M, Chen X, Rajabipour F, Hendrickson CT (2014) Comparative life cycle assessment of conventional, glass powder, and alkali-activated slag concrete and mortar. J Infrastruct Syst 20(4):04014020. https://doi.org/10.1061/(ASCE)IS.1943-555X.0000211
12. Gomaa E, Han T, ElGawady M, Huang J, Kumar A (2021) Machine learning to predict properties of fresh and hardened alkali-activated concrete. Cem Concr Compos 115:103863. https://doi.org/10.1016/j.cemconcomp.2020.103863
13. Wardhono A, Gunasekara C, Law DW, Setunge S (2017) Comparison of long term performance between alkali activated slag and fly ash geopolymer concretes. Constr Build Mater 143:272–279. https://doi.org/10.1016/j.conbuildmat.2017.03.153
14. Wang GM, Ma Y (2018) Drying shrinkage of alkali-activated fly ash/slag blended system. J Sustain Cem Based

Mater 7(203):213. https://doi.org/10.1080/21650373.2018.1471424
15. Hammad N, El-Nemr A, El-Deen Hasan H (2021) The performance of fiber GGBFS based alkali-activated concrete. J Build Eng 42:102464. https://doi.org/10.1016/j.jobe.2021.102464
16. Puertas F, Gil-Maroto A, Palacios M, Amat T (2006) Alkali-activated slag mortars reinforced with ar glassfibre. Performance and properties. Mater Constr 56(283):79–90. https://doi.org/10.3989/mc.2006.v56.i283.10
17. Adesina A (2020) Performance of fibre reinforced alkali-activated composites—a review. Materialia 12:100782. https://doi.org/10.1016/j.mtla.2020.100782
18. Chen W, Xie Y, Li B, Li B, Wang J, Thom N (2021) Role of aggregate and fibre in strength and drying shrinkage of alkali-activated slag mortar. Constr Build Mater 299:124002. https://doi.org/10.1016/j.conbuildmat.2021.124002
19. Wu Y-F (2004) The effect of longitudinal reinforcement on the cyclic shear behavior of glass fiber reinforced gypsum wall panels: tests. Eng Struct 26(11):1633–1646. https://doi.org/10.1016/j.engstruct.2004.06.009
20. Enfedaque A, Cendón D, Gálvez F, Sánchez-Gálvez V (2010) Analysis of glass fiber reinforced cement (GRC) fracture surfaces. Constr Build Mater 24(7):1302–1308. https://doi.org/10.1016/j.conbuildmat.2009.12.005
21. Enfedaque A, Cendón D, Gálvez F, Sánchez-Gálvez V (2011) Failure and impact behavior of facade panels made of glass fiber reinforced cement (GRC). Eng Fail Anal 18(7):1652–1663. https://doi.org/10.1016/j.engfailanal.2011.01.004
22. Chen Y, Qiao P (2011) Crack growth resistance of hybrid fiber-reinforced cement matrix composites. J Aerosp Eng 24(2):154–161. https://doi.org/10.1061/(asce)as.1943-5525.0000031
23. Li B, Yu S, Gao B, Li Y, Wu F, Xia D, Chi Y, Wang S (2023) Effect of recycled aggregate and steel fiber contents on the mechanical properties and sustainability aspects of alkali-activated slag-based concrete. J Build Eng 66:105939. https://doi.org/10.1016/j.jobe.2023.105939
24. Thunuguntla CS, Gunneswara Rao TD (2018) Effect of mix design parameters on mechanical and durability properties of alkali activated slag concrete. Constr Build Mater 193:173–188. https://doi.org/10.1016/j.conbuildmat.2018.10.189
25. Perera DS, Uchida O, Vance ER, Finnie KS (2007) Influence of curing schedule on the integrity of geopolymers. J Mater Sci 42(9):3099–3106. https://doi.org/10.1007/s10853-006-0533-6
26. Wang Y, Montanari L, Jason Weiss W, Suraneni P (2020) Internal curing using superabsorbent polymers for alkali activated slag-fly ash mixtures. In: Boshoff WP, Combrinck R, Mechtcherine V, Wyrzykowski M (eds) 3rd international conference on the application of superabsorbent polymers (SAP) and other new admixtures towards smart concrete, vol 24. Springer International Publishing, RILEM Bookseries, Cham, pp 239–247. https://doi.org/10.1007/978-3-030-33342-3_26
27. Gao X, Yu QL, Brouwers HJH (2016) Assessing the porosity and shrinkage of alkali activated slag-fly ash composites designed applying a packing model. Constr Build Mater 119:175–184. https://doi.org/10.1016/j.conbuildmat.2016.05.026
28. Bernal S, De Gutierrez R, Delvasto S, Rodriguez E (2010) Performance of an alkali-activated slag concrete reinforced with steel fibers. Constr Build Mater 24(2):208–214. https://doi.org/10.1016/j.conbuildmat.2007.10.027
29. Koenig A, Wuestemann A, Gatti F, Rossi L, Fuchs F, Fessel D, Dathe F, Dehn F, Minelli F (2019) Flexural behaviour of steel and macro-PP fibre reinforced concretes based on alkali-activated binders. Constr Build Mater 211:583–593. https://doi.org/10.1016/j.conbuildmat.2019.03.227
30. Nematollahi B, Sanjayan J, Ahmed Shaikh Faiz U (2015) Tensile strain hardening behavior of PVA fiber-reinforced engineered geopolymer composite. J Mater Civ Eng 27(10):04015001. https://doi.org/10.1061/(ASCE)MT.1943-5533.0001242
31. Bhutta A, Farooq M, Banthia N (2019) Performance characteristics of micro fiber-reinforced geopolymer mortars for repair. Constr Build Mater 215:605–612. https://doi.org/10.1016/j.conbuildmat.2019.04.210
32. Alomayri T (2017) Effect of glass microfibre addition on the mechanical performances of fly ash-based geopolymer composites. J Asian Ceram Soc 5(3):334–340. https://doi.org/10.1016/j.jascer.2017.06.007
33. Ahmed SFU, Mihashi H (2011) Strain hardening behavior of lightweight hybrid polyvinyl alcohol (PVA) fiber reinforced cement composites. Mater Struct 44(6):1179–1191. https://doi.org/10.1617/s11527-010-9691-8
34. Aydın S, Baradan B (2013) The effect of fiber properties on high performance alkali-activated slag/silica fume mortars. Compos B Eng 45(1):63–69. https://doi.org/10.1016/j.compositesb.2012.09.080
35. Shah SFA, Chen B, Oderji SY, Aminul Haque M, Ahmad MR (2020) Comparative study on the effect of fiber type and content on the performance of one-part alkali-activated mortar. Constr Build Mater 243:118221. https://doi.org/10.1016/j.conbuildmat.2020.118221
36. Hossain KMA, Lachemi M, Sammour M, Sonebi M (2012) Influence of polyvinyl alcohol, steel, and hybrid fibers on fresh and rheological properties of self-consolidating concrete. J Mater Civ Eng 24(9):1211–1220. https://doi.org/10.1061/(ASCE)MT.1943-5533.0000490
37. Midhuna MS, GunneswaraRao TD, Chaitanya Srikrishna T (2018) Mechanical and fracture properties of glass fiber reinforced geopolymer concrete. Adv Concr Constr 6(1):29–45. https://doi.org/10.12989/acc.2018.6.1.029
38. Puertas F, Amat T, Fernández-Jiménez A, Vázquez T (2003) Mechanical and durable behaviour of alkaline cement mortars reinforced with polypropylene fibres. Cem Concr Res 33(12):2031–2036. https://doi.org/10.1016/S0008-8846(03)00222-9
39. Ranjbar N, Zhang M (2020) Fiber-reinforced geopolymer composites: a review. Cem Concr Compos 107:103498. https://doi.org/10.1016/j.cemconcomp.2019.103498
40. Rossi L, Miranda de Lima L, Sun Y, Dehn F, Provis JL, Ye G, De Schutter G (2022) Future perspectives for alkali-activated materials: from existing standards to structural applications. RILEM Tech Lett 7:159–177

41. El-Hassan H, Elkholy S (2019) Performance evaluation and microstructure characterization of steel fiber–reinforced alkali-activated slag concrete incorporating fly ash. J Mater Civ Eng 31(10):04019223. https://doi.org/10.1061/(asce)mt.1943-5533.0002872
42. Afroughsabet V, Ozbakkaloglu T (2015) Mechanical and durability properties of high-strength concrete containing steel and polypropylene fibers. Constr Build Mater 94:73–82. https://doi.org/10.1016/j.conbuildmat.2015.06.051
43. Deng Z, Yang Z, Bian J, Lin J, Long Z, Hong G, Yang Z, Ye Y (2022) Advantages and disadvantages of PVA-fibre-reinforced slag- and fly ash-blended geopolymer composites: engineering properties and microstructure. Constr Build Mater 349:128690. https://doi.org/10.1016/j.conbuildmat.2022.128690
44. Rossi L, Patel RA, Dehn F (2025) New analytical models to predict the mechanical performance of steel fiber-reinforced alkali-activated concrete. Struct Concr 26(1):236–247. https://doi.org/10.1002/suco.202301104
45. El-Hassan H, Medljy J, El-Maaddawy T (2021) Properties of steel fiber-reinforced alkali-activated slag concrete made with recycled concrete aggregates and dune sand. Sustainability. https://doi.org/10.3390/su13148017
46. Noushini A, Hastings M, Castel A, Aslani F (2018) Mechanical and flexural performance of synthetic fibre reinforced geopolymer concrete. Constr Build Mater 186:454–475. https://doi.org/10.1016/j.conbuildmat.2018.07.110
47. Yang S, Zhao R, Ma B, Si R, Zeng X (2023) Mechanical and fracture properties of fly ash-based geopolymer concrete with different fibers. J Build Eng 63:105281. https://doi.org/10.1016/j.jobe.2022.105281
48. Abdulkareem M, Havukainen J, Horttanainen M (2019) How environmentally sustainable are fibre reinforced alkali-activated concretes? J Clean Prod 236:117601. https://doi.org/10.1016/j.jclepro.2019.07.076
49. EN 1097-6 (2014) Tests for mechanical and physical properties of aggregate. Determination of particle density and water absorption. European Committee for Standardization (CEN)
50. Geosil ® 34417 Alkaline activator based on sodium silicate (technical sheet). https://www.woellner.de/files/downloads/TDS/TDS-Geosil_34417-GB.pdf. Accessed on 2 Oct 2024
51. BS 8500-1 (2015) Complementary British Standard to BS EN 206. Part 1, method of specifying and guidance for the specifier. UK
52. Chottemada PG, Mishra A, Thomas RJ, Kar A (2024) Evaluation of long-term properties and life cycle assessment of alkali-activated concrete with varying fiber inclusions. Constr Build Mater 431:136437. https://doi.org/10.1016/j.conbuildmat.2024.136437
53. Kara De Maeijer P, Ye G, Li Z, Ramagiri KK, De Schutter G, Sun Y, Dehn F, Kar A, Yliniemi J, Ma Y, Ichimiya K, Masi G, Phung QT, Sha W. Examining reproducible mix design, fresh and mechanical properties of ground granulated blast furnace slag-based alkali-activated concrete (GGBFS-based AAC): results of an interlaboratory study of RILEM TC 294-MPA. Mater Struct. (in submission)
54. EN 12350-2 (2019) Testing fresh concrete—part 2: slump test. European Committee for Standardization (CEN), Brussels, Belgium
55. EN 12390-1 (2022) Testing hardened concrete—part 1: shape, dimensions and other. European Committee for Standardization (CEN)
56. EN 12390-7:2019/AC:2020 Testing hardened concrete—part 7: density of hardened concrete. European Committee for Standardization (CEN), Brussels, Belgium
57. EN 12390-3 (2019) Testing hardened concrete—part 3: compressive strength of test specimens. European Committee for Standardization (CEN), Brussels, Belgium
58. EN 12390-6. Testing hardened concrete part 6: tensile splitting strength of test specimens. European Committee for Standardization (CEN), Brussels, Belgium
59. LVS 156-1:2022 Concrete (2023) Latvian National Annex to European Standard EN 206 'Concrete. Technical provisions, performance, manufacture and compliance'/ Betons. Latvijas nacionālais pielikums Eiropas standartam EN 206 'Betons. Tehniskie noteikumi, darbu izpildījums, ražošana un atbilstība' (in Latvian), Cabinet of Ministers, Latvia
60. Amran M, Fediuk R, Abdelgader HS, Murali G, Ozbakkaloglu T, Lee YH, Lee YY (2022) Fiber-reinforced alkali-activated concrete: a review. J Build Eng 45:103638. https://doi.org/10.1016/j.jobe.2021.103638